Topology changes in fluid membranes

David H. Boal and Madan Rao
Department of Physics, Simon Fraser University, Burnaby, British Columbia, Canada V5A 1S6
(Received 18 February 1992)

Shape changes of a fluid membrane with fixed area modeled by a curvature Hamiltonian and a boundary line tension are investigated. The zero-temperature energetics are studied using a variational principle in the space of axisymmetric shapes. For zero spontaneous curvature, the only energy minimizing shapes are the disk and the sphere. The energy barrier heights between these configurations are determined as a function of the Hamiltonian parameters. Thermal fluctuations of the shape are studied by means of a Monte Carlo simulation. The "phase transition" from open to closed topology is determined as a function of the rigidity and line tension at nonzero temperature. The transition is found to persist even at zero membrane rigidity. The energetics of the transition are shown to be related to the branched polymer scaling behavior of the fluid membrane.

PACS number(s): 05.40.+j, 82.65.Dp, 64.70.−p, 87.22.Bt

I. INTRODUCTION

The properties of fluid membranes have application to fields ranging from biology to particle physics [1]. Biological examples include lipid bilayer membranes which spontaneously self-aggregate in aqueous solution to form closed two-dimensional surfaces [2,3]. Open bilayer configurations can be stabilized by introducing edge-reactant salts [4,5]. Closed vesicles with spherical [3] and toroidal [6] topology have been studied experimentally. From the theoretical point of view, biological systems are low-temperature systems in the sense that the bending energy scale is many times $k_B T$, where T is the temperature and k_B is Boltzmann's constant. Hence, many theoretical studies [7–12] have been carried out to determine the energy minimizing (zero-temperature) shapes of axially symmetric vesicles with fixed topology in three dimensions subject to the constraints of constant surface area and enclosed volume.

At finite temperature, computer simulations and other studies of closed surfaces have been performed for rings embedded in two dimensions [13–16] and surfaces embedded in three dimensions [17–27]. Of particular interest in elementary particle physics are the properties of random surfaces, which may play a role as regularizers of string theory [26–31]. While particle physics research first focused on infinite-temperature surfaces, interest has since broadened to include finite-temperature properties as well.

A model for the energy of an open fluid membrane based upon the so-called spontaneous curvature model [7] is

$$E[S]=(\kappa_c/2)\int dA\,(C_1+C_2-C_0)^2 + \kappa_g\int dA\,(C_1C_2)+\lambda\int d\Gamma\ . \tag{1}$$

In the above expression, C_1 and C_2 are the local principal curvatures and the parameter C_0 is the spontaneous curvature. For closed topologies, the integral over the Gaussian curvature C_1C_2 is equal to a (topology-dependent) constant, independent of the configuration. The bending elastic coefficients are κ_c and κ_g. The last term is the line tension energy and is proportional to the perimeter of the boundary $\int d\Gamma$. In biomembranes, the line tension modulus [4,5] originates from the interactions of the amphiphilic molecules at the edge of a bilayer.

The parameters which appear in Eq. (1) are "effective" parameters appropriate for mesoscopic problems. They may not be similar to values which apply to microscopic (molecular) phenomena. In biological systems, lipid molecules may relax on a molecular scale at the edges of a membrane sheet, thus modifying the effective line tension. Thus, the numerical values of the model parameters appearing here may not be simultaneously applicable to lipid bilayers and microemulsions, for example [32].

The origin of the spontaneous curvature term C_0 in biomembranes has been investigated by a number of authors, a recent summary can be found in Ref. [33]. An alternate model Hamiltonian for bilayer systems is the bilayer coupling model [8], which maintains a constant area difference between the monolayers. Neither model describes all of the shape change features of biomembranes, and a true description may involve a hybrid of the two models [34].

In this paper we investigate the characteristics of open and closed membrane configurations, and the transition between them, in three dimensions. The transition is driven by the line tension λ. In Sec. II we determine the ground-state (zero-temperature) configurations. We show that there is a first-order transition between the open and closed topologies. For some regions of parameter space, one topology is metastable with respect to the other. We solve a set of Euler equations to determine the energy barrier between the topologies by assuming that the barrier has axial symmetry.

In Sec. III a Monte Carlo simulation is introduced to determine the nature of the transition at nonzero temperature. A novel feature of the simulation is that it allows

changes between open and closed topologies. Sample configurations of the open and closed topologies taken from the simulation are shown in Fig. 1. We show that the transition persists even at zero bending rigidity. We also find that the branched polymer scaling of the vesicle shape determines the value of the line tension required to close the membrane at zero rigidity. Finally, our conclusions are summarized in Sec. IV.

II. GROUND-STATE CONFIGURATIONS

We begin our discussion of open vesicle ground states by considering spherical-cap configurations in Sec. II A. Spherical-cap configurations, which are axisymmetric configurations with a constant radius of curvature, have been used previously to estimate open membrane energetics [4,5,35]. In Sec. II B we relax the constant-curvature condition and examine the general problem of axisymmetric shapes. We find that the ground-state configurations are extreme spherical-cap configurations—either the disk or the sphere. However, the intermediate spherical-cap configurations are shown to overestimate the energy barrier between metastable and ground states compared to the barriers found for general axisymmetric shapes.

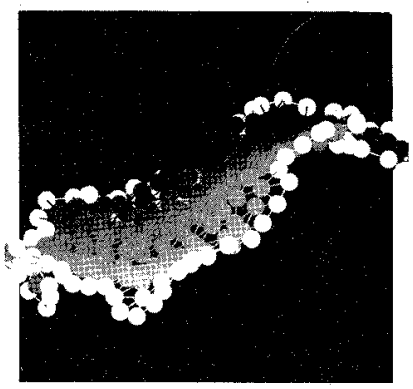

(a)

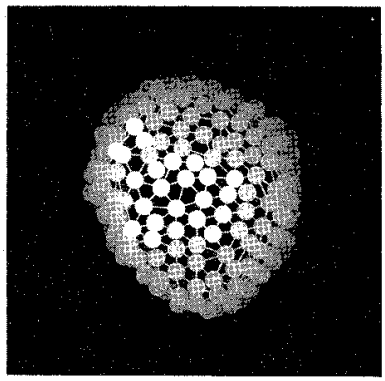

(b)

FIG. 1. Simulated membrane configurations at low temperature showing open (a) and closed (b) topology. The white beads lie along the edge of the membrane.

A. Spherical-cap configurations

Our zero-temperature investigation begins with a variational study of a restricted set of "spherical-cap" configurations. The configurations have a constant curvature C, and boundary radius r. The area of a spherical cap is thus

$$A = 2\pi C^{-2}[1 \pm (1 - C^2 r^2)^{1/2}] , \tag{2}$$

where the choice of sign depends on the position of the boundary with respect to the center of curvature. It is generally useful to work in terms of reduced quantities $R \equiv r A^{-1/2}$ and $\Lambda \equiv \lambda A^{1/2}$.

In this section, we confine our analysis to zero spontaneous curvature $C_0 = 0$, for which the energy of a spherical cap is

$$E_{\text{cap}} = 4\pi(1 - \pi R^2)(2\kappa_c + \kappa_g) + 2\pi\Lambda R . \tag{3}$$

The disk ($R = \pi^{-1/2}$) and the sphere ($R = 0$) are at the boundary of the space of spherical-cap configurations and at least one of their energies is lower than that of any other shape in this space. Tuning a parameter $\alpha \equiv \Lambda / [4\pi^{1/2}(2\kappa_c + \kappa_g)]$, we find that $\alpha = \frac{1}{2}$ represents a "phase transition" between an open disk ($\alpha \leq \frac{1}{2}$) and a closed sphere ($\alpha \geq \frac{1}{2}$). These results have been presented previously using different parametrizations [4,5,35].

This first-order phase transition corresponds to a topology changing transition. The jump in the perimeter (for finite area) is given by $(4\pi A)^{1/2}$. For $0 \leq \alpha \leq 1$ one of the disk or sphere configurations is metastable in the space of spherical caps. The energy barrier heights from the sphere and the disk configurations are $\Delta E_{\text{sphere}} = 4\pi\alpha^2(2\kappa_c + \kappa_g)$ and $\Delta E_{\text{disk}} = 4\pi(\alpha - 1)^2(2\kappa_c + \kappa_g)$, respectively. These results are summarized in Fig. 2, which shows the energy of the sphere and disk

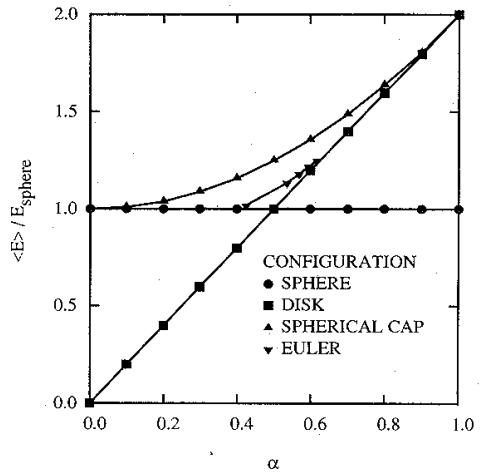

FIG. 2. Energetics of the ground-state configurations, given in terms of the ground-state sphere energy. The barrier energies are shown for both spherical-cap and Euler equation solutions.

configurations, and the barrier height between them, as a function of α. The energies are normalized to the energy of a sphere $E_{\text{sphere}}=4\pi(2\kappa_c+\kappa_g)$. The figure shows both the barrier height for spherical-cap configurations and also the barrier predicted by the Euler equation solutions which are described in the following section. It can be seen from the figure that the spherical-cap barrier heights cannot be used reliably to estimate passage times between boundary shapes because spherical-cap calculations significantly overestimate the barrier heights obtained from a more general variational principle.

B. Axisymmetric configurations

We now extend our variational analysis to include a larger class of two-dimensional surfaces, namely surfaces of revolution. The zero-temperature equilibrium shape of the membrane is obtained [7] by minimizing the energy functional (1) subject to a constant area constraint. This is done by introducing the "free-energy" functional

$$\Phi[S]=E[S]+\sigma A[S] , \tag{4}$$

where σ ("surface tension") is a Lagrange multiplier introduced to fix the area.

Since we are dealing with equilibrium shapes of a simply connected open membrane, the boundary must be varied in considering variations of Φ. Axisymmetric simply connected open surfaces can be generated by rotating a curve $z(x)$ about the z axis, where (x,z) form an orthogonal coordinate system. However, it is more convenient to use the arc length s as the independent variable describing the curve, since it is monotonic in x. The free-energy functional written in terms of s is

$$\begin{aligned}\Phi[S]=&\pi\kappa_c\int x(\sin\theta/x+\theta'-C_0)^2ds\\&+2\pi\kappa_g\int\theta'\sin\theta\,ds+2\pi\sigma\int x\,ds+2\pi\lambda\int x'ds\\&+\int\mu(x'-\cos\theta)ds ,\end{aligned} \tag{5}$$

where θ is the angle which the tangent to the curve makes with respect to the x axis. The integrals are evaluated along the arc length to its maximum value s_m. Primes beside a symbol indicate derivatives with respect to s. The Lagrange multiplier μ is introduced to enforce the condition

$$x'=\cos\theta \tag{6}$$

and varies along the arc with s.

In terms of the arc length s, variation of Eq. (5) yields the same set of nonlinear autonomous Euler equations as are obtained for closed vesicles [7] at zero pressure. Three equations which allow one to integrate the set of variables x, θ, and μ from their initial values at $s=0$ are Eq. (6) plus the Euler equations

$$\mu'=\pi\kappa_c(\theta'-C_0)^2-\pi\kappa_c\sin^2\theta/x^2+2\pi\sigma , \tag{7}$$

$$\theta''=\sin\theta\cos\theta/x^2+\mu\sin\theta/(2\pi\kappa_c x)-\theta'\cos\theta/x . \tag{8}$$

Variation of the boundary (s_m) gives rise to a set of "natural boundary conditions" which the Euler solutions must satisfy (κ_g has been set equal to zero, for convenience),

$$x(s_m)=0 \quad \text{or} \quad C_1(s_m)+C_2(s_m)=C_0 , \tag{9}$$

$$\sigma x(s_m)+\lambda dx/ds(s=s_m)=0 , \tag{10}$$

and

$$\mu(s_m)=-2\pi\lambda . \tag{11}$$

The numerical procedure we use for constructing solutions is as follows. The coordinate system is chosen such that $x(s=0)=0$ and $\theta(s=0)=0$. Values are chosen for two of the other quantities [for example, $\mu(s=0)$ and $\theta'(s=0)$] and Eqs. (6)–(8) are used to integrate the values of x, θ, and μ. The integration stops at s_m, determined by Eq. (11). The solution is checked against the constraints (9) and (10), and the procedure repeated with a new initialization until Eqs. (9) and (10) are satisfied to a chosen accuracy. The configuration area A is then an outcome of the value chosen for σ. Obviously, there are many variants of the above procedure, depending on which variable is of greatest interest. However, one can always rescale the solution parameters to find a particular value of a chosen observable. For example, the solution set (C, s_m, λ, and σ) for area A is related to the set (C^*, s_m^*, λ^*, and σ^*) for area $A^*=\rho^2A$ via

$$C^*=C/\rho,\quad S_m^*=\rho S_m,\quad \lambda^*=\lambda/\rho,\quad \sigma^*=\sigma/\rho^2 , \tag{12}$$

where C is one of the curvatures. For the remainder of this section, λ, σ, and μ are expressed in units of κ_c, as suggested by Eqs. (7)–(11).

For each of the j Euler solutions that satisfy the above boundary conditions, one can construct an "energy sheet" $E_j(A,\lambda)$. It is clear that these Euler-shape sheets are only a subset of all axisymmetric-shape sheets, which include boundary shapes like disks, spheres, and multispheres. The ground state is the lowest-energy sheet at

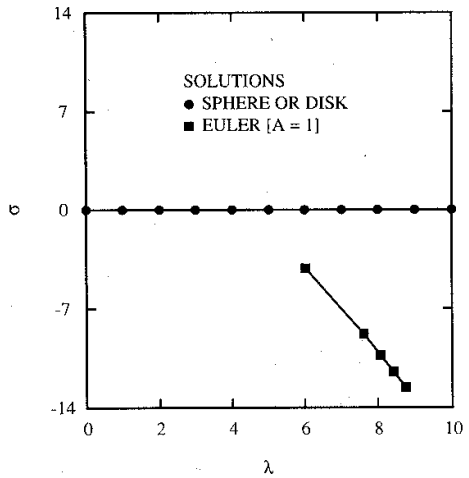

FIG. 3. Partial parameter set for solutions to Euler equations with area $A=1$ and $\kappa_g=0$. The quantities λ and σ are quoted in units of κ_c.

each point (A,λ). Our "phase diagram" in the (A,λ) plane should append smoothly onto the zero-pressure line of the phase diagram for closed membranes [7–10]. Once the surface closes, there may be an additional constraint keeping the enclosed volume fixed.

Let us analyze the $C_0=0$ solutions first. The boundary condition Eq. (9) implies that the only spherical caps which are Euler solutions are disks or spheres. It is easy to see that spheres of any radius are Euler solutions when $\sigma=0$. This is a consequence of the scale invariance of the Hamiltonian. We can further show that if $\lambda=0$, then the only Euler solution is a disk. From a numerical solution of the Euler equations, we are able to find axisymmetric solutions consistent with the boundary conditions (9) and (10) for $\sigma\leq 0$ and $\lambda\geq 0$. A partial solution set corresponding to $A+1$ is shown in Fig. 3. Other than the sphere and disk, these configurations are not ground states but are the minimum energy states for passing between the disk and the sphere.

Except for the boundary shapes, the Euler solutions are not the same as the spherical-cap configurations. Two sample solutions are shown in Fig. 4. One can see the tendency of the boundary to curve away from the axis of symmetry in both solutions, whereas the spherical-cap configurations have the same curvature at the boundary as they do in the "interior" of the solution. The appearance of the Euler solution boundaries is a reflection of Eqs. (9) and (10).

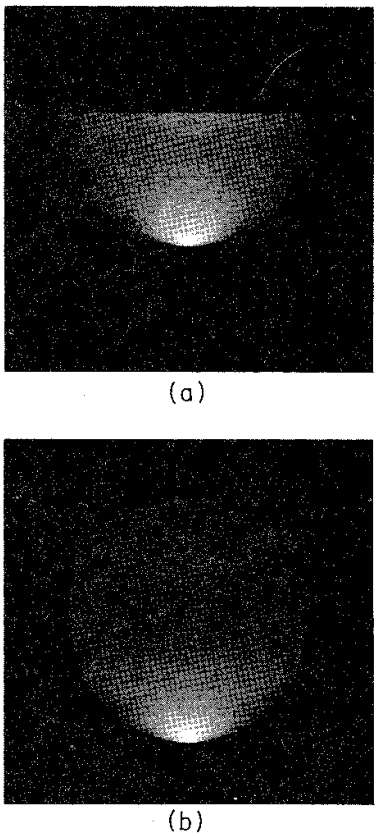

FIG. 4. Sample solutions to the Euler equations for $A=1$, $\kappa_g=0$, and (λ,σ,s_m) of $(8.75,-12.53,0.63)$ for (a) and $(6.02,-4.09,0.79)$ for (b). The curvature of the solution near the open boundary is opposite to that obtained for spherical caps. The quantities λ and σ are quoted in units of κ_c.

The energies of the Euler solutions are shown in Fig. 2, in which an Euler solution for a given area is compared with a spherical cap of the same area. The energy barrier between the sphere and the disk configurations is substantially lower than what is obtained from spherical caps. In fact, there are some regions of parameter space where a configuration is metastable in the space of spherical caps but unstable or marginally stable in the space of Euler solutions. The spherical configuration for α less than about 0.3 and the disk configuration for α greater than about 0.7 appear to be unstable in the space of Euler shapes, to our numerical accuracy.

Hence, the transit time for decay of a given metastable configuration is overestimated if a spherical-cap configuration is used for the energy barrier height. For example, the maximum barrier in both solutions sets is at $\alpha=\frac{1}{2}$. Suppose we use the usual Kramers argument to estimate the decay of a metastable state as the product of an attempt rate times $\exp(-\beta\Delta E)$ where ΔE is the barrier height. Assuming $\beta\kappa_c=20$ for a lipid bilayer, then the Euler shape lifetime at $\alpha=\frac{1}{2}$ is lower by a factor of e^{-75} compared to the spherical-cap lifetime.

When $C_0\neq 0$, the condition for a section of a sphere to be an Euler solution is that the radius R_{sphere} of the sphere should satisfy

$$(C_0^2+2\sigma)/2C_0=R_{\text{sphere}}^{-1}\ . \tag{13}$$

This obeys the boundary conditions Eqs. (9) and (10) only at $\lambda=\sigma=0$ (where a spherical cap with radius $2/C_0$ has zero free energy Φ). Spherical solutions [whose radius R_{sphere} is given by Eq. (13)] exist at all values of σ. Multiple sphere configurations with the radius of each sphere given by Eq. (13) exist at $\sigma=0$ (this is a consequence of the "kissing condition" defined in Refs. [9] and [10]). For closed surfaces with σ fixed, there exists only one length scale; thus all the spheres in the multiplet have the same radius.

If we fix the area at $4n\pi(2/C_0)^2\equiv nA_H$, where n is an integer, then the membrane will spontaneously form n multiplet Helfrich spheres of radius $2/C_0$ with zero (infinitesimal) neck radius. This costs no energy [9] and is therefore the ground state (for positive λ). Thus as A increases, Helfrich spheres are sprouted out periodically with period A_H.

III. SIMULATIONS AT FINITE TEMPERATURE

A. Monte Carlo model

In Sec. II we show that for a given fixed area A and fixed rigidity κ_c, the disk is a lowest-energy solution for $\lambda<\lambda_c=4\kappa_c(\pi/A)^{1/2}$, where there is a "first-order transition" to a sphere (which is the ground state beyond λ_c). At nonzero temperatures, the transition to closed topology has to overcome the entropy associated with fluctua-

tions of the membrane boundary. We investigate this finite-temperature topological transition using a Monte Carlo simulation.

In our simulations, the membrane is treated as a two-dimensional, self-avoiding, tethered manifold consisting of hard spherical beads (vertices) linked together by flexible tethers (bonds). The fixed connectivity tethered model developed for the study of elastic membranes [17] is inappropriate for the study of fluid membranes. Baumgartner and Ho [20] have developed an algorithm for bond reconnection which simulates a fluid membrane of fixed topology. Here, we introduce a bond creation and removal algorithm (described briefly in [23]) which allows for topology changes in the fluid membrane.

In our simulations, the number of vertices N is fixed but the number of bonds is not. Because of the tethers, the total membrane area is not a constant and can change by up to 50% around the mean. Vertices which define the edge of the sheet are called external, as are bonds linking two external vertices. All other vertices and bonds are internal. Corresponding to Eq. (1), we use the discretized Hamiltonian

$$H = k_{\rm rig} \sum_{i,j} (1 - \mathbf{n}_i \cdot \mathbf{n}_j) + k_{\rm ten} P \ , \tag{14}$$

where each $\mathbf{n}$ is a unit vector normal to the plaquette plane formed by three vertices which are all nearest neighbor to each other. The sum is over plaquettes i and j which share a common tether. The perimeter P is a sum over the distance between nearest-neighbor external vertices. In addition to Eq. (14), the vertices are subject to potentials which enforce the self-avoidance constraint: the vertices are infinitely repulsive at distances less than the bead diameter a (for all vertex pairs) or greater than $\sqrt{3}a$ (for vertices connected by tethers). In the continuum limit, the tension parameter $k_{\rm ten}$ corresponds to λ and the energy of a sphere is equal to $4\pi k_{\rm rig}/\sqrt{3}$ (in terms of the discrete rigidity parameter $k_{\rm rig}$) or $4\pi(2\kappa_c + \kappa_g)$ (continuum).

A set of appropriately weighted sample configurations is generated using the usual Metropolis Monte Carlo technique in which trial moves are made on the vertex positions and connectivity. A sweep across the membrane involves the following steps: (i) An attempt is made to change the position of each vertex (sequentially by vertex label) by choosing a new position randomly from within a cubic box of length $2l$ to the side centered on the old position. (ii) An attempt is made to reconnect every internal bond. Each bond is defined by its two end vertices v_1 and v_2, and its two "opposite" vertices v_a and v_b. The move consists of reconnecting the bond to v_a and v_b with v_1 and v_2 becoming the new "opposite" vertices. (iii) An attempt is made to remove each external bond (which defines the boundary), reducing the total number of bonds by one while converting two internal bonds into external bonds. This procedure has the effect of increasing the perimeter. (iv) An attempt is made to convert each external vertex into an internal vertex by adding a new external bond directly between its two external nearest neighbors. This move decreases the perimeter since two external bonds are made into internal bonds, reducing the total number of external bonds by one. Our simulation forbids the total number of external bonds from decreasing below four, so that we can observe the evolution of the boundary.

Each trial move in (i)–(iv) is accepted or rejected according to the Boltzmann weight $\exp(-\beta\Delta H)$, where β is the inverse temperature and ΔH is the energy change associated with the move from Eq. (14). Procedure (ii) was introduced by Baumgartner and Ho [20] to simulate fluid membranes, while procedures (iii) and (iv) are new. In procedures (ii)–(iv), the connectivity of any vertex is not allowed to decrease below 3 or increase above 9. Further, connectivity checks are made to ensure that the membrane retains the simple connectivity of a single sheet: remote parts of the sheet are not allowed to become connected nor are holes allowed to develop in the sheet. We accomplish this by forbidding a given bond to be shared by more than two triangles defining the membrane surface. This implies that all triangles defined by nearest-neighbor vertices exist on the surface of the membrane, and that the surface is determined completely by such triangles.

Two sample configurations are shown in Fig. 1 for rigidity $\kappa_{\rm rig}=8$, where we define $\kappa_{\rm rig}\equiv\beta k_{\rm rig}$ and $\kappa_{\rm ten}\equiv\beta k_{\rm ten}$. We emphasize that $\kappa_{\rm rig}$ and $\kappa_{\rm ten}$ (discrete) contain the inverse temperature whereas κ_c, κ_g, and λ (continuum) do not. A total of 100 sample configurations is generated at each $(\kappa_{\rm rig},\kappa_{\rm ten})$ combination. Each configuration is separated by a "Rouse time" $\tau = N/l^2$ Monte Carlo sweeps, where we use $l = 0.1$. Before sample collection, each initialization is allowed to relax for 10τ. For the lowest temperatures ($\kappa_{\rm rig}=2$) we check that both open and closed membrane initializations reach the same equilibrium configurations. For $\kappa_{\rm rig}=4$, equilibrium may not be reached near the transition point for much longer than 10τ.

B. Topology change at $T > 0$

With our Hamiltonian and discretization, the zero-temperature topology transition occurs at $K(N) \equiv \sqrt{3}[P(N)/4\pi][\kappa_{\rm ten}/\kappa_{\rm rig}] = 1$, which is the discrete equivalent of $\alpha = \frac{1}{2}$ in Sec. II A. Because of the system size and connectivity, we use $P(N) = (12N-3)^{1/2} - 3$ of a hexagon as a reference perimeter which is less than 5% different from an equivalent disk perimeter. The behavior found in the simulations at moderate temperature, $1/\kappa_{\rm rig} = \frac{1}{2}$, is shown in Fig. 5. One can see that the average perimeter $\langle P \rangle$, drops sharply to a value of $4a$ as a function of $\kappa_{\rm ten}$. In Fig. 5, $\langle P \rangle$ has been divided by $P(N)$ to show the similarity of the change as a function of N. The transition does not occur precisely at $K(N)=1$ because of finite-temperature fluctuations.

Finite-temperature effects show up in two different ways in Fig. 5. The first is the magnitude of the change in perimeter ΔP at the transition point. If the open membrane looks like a circular disk near the transition point, then we would expect $\Delta P \approx N^{1/2}$. However, Fig. 5 clearly shows that the scaling of ΔP is much closer to N^1 than $N^{1/2}$ [recall that the reference perimeter $P(N)$ scales like

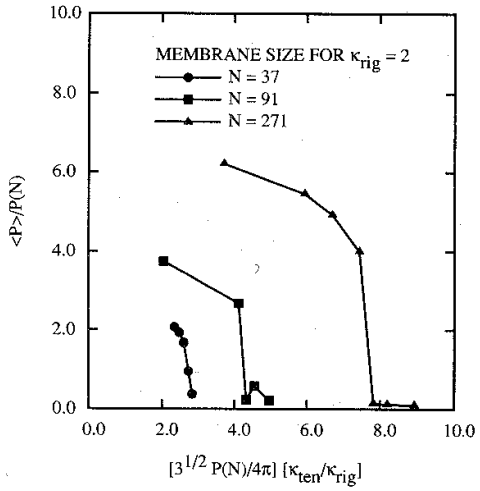

FIG. 5. Expectation of the scaled perimeter $\langle P\rangle/P(N)$ shown as a function of the scaled line tension $\sqrt{3}[P(N)/4\pi][\kappa_{ten}/\kappa_{rig}]$. See text for definition of symbols. The perimeter is shown for $\kappa_{rig}=2$ and $N=37$, 91, and 271.

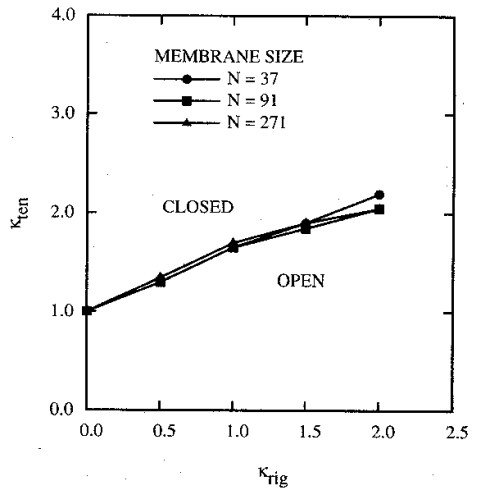

FIG. 7. Topology boundry parameters $(\kappa_{rig},\kappa_{ten})$ shown as a function of membrane size N.

$N^{1/2}$]. Other simulations [22,23,36] show that an open membrane scales like a self-avoiding branched polymer (SABP), so that far away from the transition, $P\approx N$. Thus, SABP scaling predicts that near the transition ΔP should scale like N^{δ}, with δ close to unity, and this behavior is observed in Fig. 5.

A second aspect of finite-temperature fluctuations is the magnitude of the line tension κ^{*}_{ten} required to close the membrane. From Fig. 5, $\kappa^{*}_{ten}>\kappa^{0}_{ten}$, where $\kappa^{0}_{ten}=4\pi\kappa_{rig}/[\sqrt{3}P(N)]$ is the zero-temperature value corresponding to $K(N)=1$. Further, κ^{*}_{ten} increases with N. A larger value of κ^{*}_{ten} is required at finite temperature because surface fluctuations raise the energy of the closed configuration above the energy of the sphere, $4\pi\kappa_{rig}/\sqrt{3}$. The magnitude of finite-temperature corrections to the zero-temperature boundary can be seen in Fig. 6, where $K(N)$ at the transition is plotted against $1/\kappa_{rig}$. The figure shows that the value of $K(N)$ at the transition tends towards the expected value of unity as the temperature $1/\kappa_{rig}$ vanishes, but is larger than unity at finite temperature and increases with N as expected. We return to the magnitude of these changes below.

In general, we find that the value of κ_{ten} required for membrane closure increases with κ_{rig}, as one would expect; a summary is shown in Fig. 7. Further, the transi-

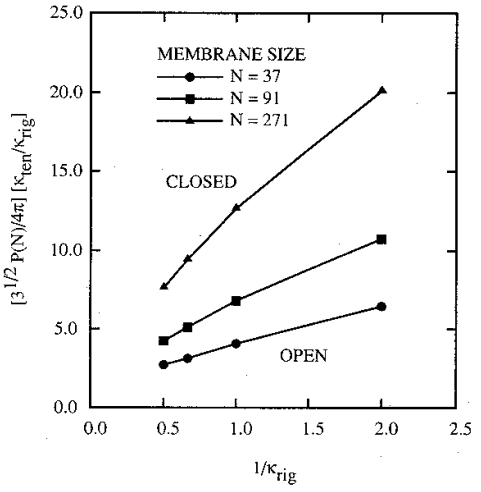

FIG. 6. Temperature dependence of topology boundary, shown as a function of N. The scaled quantity $K(N)=\sqrt{3}[P(N)/4\pi][\kappa_{ten}/\kappa_{rig}]$ at the boundary should be unity at zero temperature.

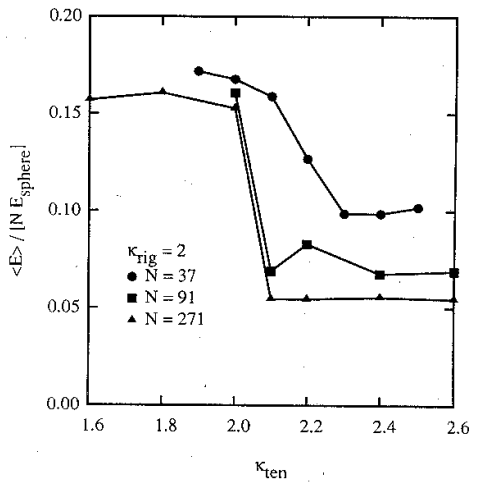

FIG. 8. Expectation of the energy as a function of line tension in the region of the open-closed transition. The energy is normalized as $\langle E\rangle/NE_{sphere}$, where E_{sphere} is the ground-state energy of the sphere.

tion is present even when κ_{rig} vanishes. At $\kappa_{rig}=0$, the line tension only has to overcome the entropy of the perimeter vertices, and we find that $\kappa^*_{ten}\approx 1$ for the transition independent of N. In the following section, we argue that this value for κ^*_{ten} can be obtained from a random surface model. The figure also shows little evidence for systematic finite-size effects at $\kappa_{rig}<1.5$.

The energy at the transition point shows a sharp change which increases with N, indicating a first-order transition. The behavior of the energy at $\kappa_{rig}=2$ is shown in Fig. 8 as an example. First note that in the figure, the energy has been normalized by the number of vertices N and the sphere energy $4\pi\kappa_{rig}/\sqrt{3}$. One sees that the decrease in $\langle E\rangle$ at the transition sharpens with increasing N, and that the magnitude of the decrease increases at least as fast as N^1. This exponent indicates that the decrease in energy is not that due to the decrease in the edge energy of a circular disk, which should scale as $N^{1/2}$. If the open membrane scales like a branched polymer right up to the transition point, then we expect $\langle P\rangle$ scales like N^1, so that $\Delta\langle E\rangle$ scales like N^1. Indeed, Fig. 5 shows that the change in the perimeter at the transition point scales more like N^1 than $N^{1/2}$. Further, the magnitude of $\Delta\langle\beta E\rangle$ from Fig. 8 is somewhat less than, but approximately equal to, $\kappa_{ten}\langle\Delta P\rangle$ obtained from Fig. 2. Hence, we conclude that the main contribution to the energy difference is from the changing edge energy, which scales like N^1.

Not only is there more edge energy than what one would expect from the ground-state disk, there is also more rigidity energy in the "bulk" of the membrane. Let us define a quantity $\epsilon\equiv(\langle\beta E\rangle-\kappa_{ten}\langle P\rangle)/E_{sphere}$ with $E_{sphere}=4\pi\kappa_{rig}/\sqrt{3}$. If the bulk energy of the closed configuration is just that of a sphere, then we expect $\epsilon=1$. For $\kappa_{rig}=2$, ϵ changes from roughly 1.5 to 2.5 across the transition point for $N=37$ and from 10 to 14 for $N=271$. In other words, the bulk energy of the open membrane is more than just $\kappa_{ten}\langle P\rangle$, and it costs more energy to close up the vesicle than simply E_{sphere}.

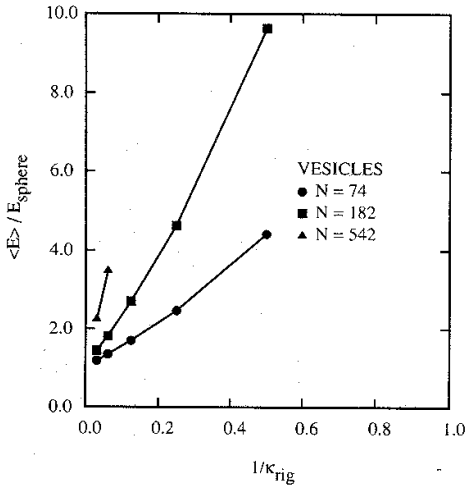

FIG. 9. Energy of a closed vesicle with the topology of a sphere as a function of the rigidity. The energy is compared with the ground-state energy of a sphere.

The variation of the bulk rigidity energy with temperature is shown in Fig. 9 for a completely closed vesicle. For temperature $1/\kappa_{rig}$ near zero, the energy of the closed configuration is close to E_{sphere}: the curves in Fig. 9 extrapolate smoothly to unity as $1/\kappa_{rig}$ goes to zero for all N. However, for the lowest temperature considered in our open membrane simulations ($\kappa_{rig}=2$), fluctuations in the membrane surface lead to energies which are much larger than E_{sphere}. The energies shown in Fig. 9 are consistent with the changes in ϵ found from Figs. 5 and 8.

C. Scaling and the topology transition

In the previous section, it is shown that κ_{ten} required to close the membrane has a value close to unity when $\kappa_{rig}=0$. This value can be obtained by considering fluctuations of the boundary and the surface. Previous work [22,23,36] has suggested that fluid membranes scale like self-avoiding branched polymers at large values of N. That is, the radius of gyration of the open or closed membranes scales like $\langle R_G^2\rangle\propto N$ and the volume of the closed vesicle scales like $\langle V\rangle\propto N$. This scale behavior is the same as that of self-avoiding random surfaces (SARS) on a lattice, which has been investigated by Glaus [25].

Glaus considers two ensembles of square plaquettes on a cubic lattice in three dimensions. One ensemble, E_1, consists of all surfaces whose boundary is in the set of single self-avoiding loops in three dimensions. This set is constructed by imposing the constraint that each plaquette shares at least one edge with a neighbor but that the surface defined by the plaquettes is self-avoiding. The second ensemble, E_2, includes all surfaces whose boundary is empty: the plaquettes used to define the surface have no free edges. At zero rigidity, our open membrane is the analog E_1 and our closed vesicle the analog of E_2.

We argue that the transition from the open to closed membrane at zero rigidity can be regarded as a competition between the entropy of a SARS model and the line tension at the boundary. Since the two phases (open and closed) coexist at the first-order point λ^*, the free energies of the two phases are equal at λ^*. At zero rigidity, the free energies are given by

$$F_{open}=\lambda\langle P\rangle-TS_{open} \tag{15a}$$

and

$$F_{closed}=-TS_{closed}\ . \tag{15b}$$

Self-avoidance terms only enter the entropic part of the free energy, since all allowed configurations are non-self-intersecting and therefore contribute zero energy.

In Glaus's simulations [25], the entropy S_{open} is given by $\ln[C_{N,1}]$, where $C_{N,1}$ is the number of configurations of a self-avoiding random surface having N plaquettes in the E_1 ensemble. This is proportional to $\mu_1^N N^{-\theta}$, where Glaus finds $\mu_1=12.798\pm0.025\pm0.018$ and $\theta=1.48\pm0.12\pm0.05$ (the first uncertainty is systematic and the second is statistical). Similarly $C_{N,2}$ is the number of configurations of a self-avoiding random surface having

N plaquettes in the E_2 ensemble. This is proportional to $\mu_2^N N^{-\phi}$. Again, Glaus finds $\mu_2 = 1.733 \pm 0.005 \pm 0.006$ and $\phi = 1.51 \pm 0.10 \pm 0.15$, the values of ϕ and θ indicating that the E_1 and E_2 ensembles belong to the same universality class.

Let us evaluate the free energies within Glaus's self-avoiding random surface (SARS) lattice model, assuming that adding a line tension does not change S_{open} but just adds $\lambda \langle P \rangle$ to the free energy as in Eq. (15a). The perimeter $\langle P \rangle = 2N$ with a 2% uncertainty in Glaus's data. To lowest order in N, the SARS model predicts $F_{\text{closed}} = -TN \ln(\mu_2)$ and $F_{\text{open}} = 2\lambda N - TN \ln(\mu_1)$. Since $F_{\text{open}} = F_{\text{closed}}$ at $\lambda^* = T\kappa_{\text{ten}}^*$, we obtain, to leading order in N, $\kappa_{\text{ten}}^* = 1.00$ with a 2% uncertainty. Within errors, this is the same value as we find in the simulation. While there are a number of assumptions involved in applying Glaus's results to ours, nevertheless the agreement is remarkable.

IV. CONCLUSION

We investigate the shapes of a fluid membrane with a curvature Hamiltonian and boundary line tension. Our zero-temperature analytical work shows that there is a sharp first-order transition between a flat disk and a spherical closed vesicle as a function of line tension. For some regions of parameter space, the sphere and disk configurations are metastable with respect to each other in the space of axially symmetric configurations. The energy barrier confining the metastable state is found to be lower in the space of axially symmetric configurations than it is in the space of spherical-cap configurations. In fact, there are some values of the line tension in which a configuration is metastable in the space of spherical-cap configurations, but unstable in the space of axially symmetric configurations. The lower barrier greatly reduces the lifetime of metastable states by factors up to the order of 10^{-30} for biomembranes.

A computer simulation is used to investigate the transition at finite temperature. The transition persists at all values of the bending rigidity and connects smoothly to the zero-temperature transition point. The behavior of the membrane energy is found to be consistent with a first-order transition at all temperatures. The transition persists at zero rigidity. Using results from a self-avoiding random surface simulation [25], the tension at the zero rigidity transition is shown to be that required to overcome the entropy of the membrane boundary. The scaling behavior of the perimeter and energy change at the transition is found to be consistent with what is expected from self-avoiding branched polymer scaling.

ACKNOWLEDGMENTS

This work is supported in part by the Natural Sciences and Engineering Research Council of Canada. We thank Udo Seifert and Michael Wortis for stimulating discussions. M. R. thanks Robert Osserman for conversations regarding isoperimetric inequalities.

[1] For a review, see *Statistical Mechanics of Membranes and Surfaces*, edited by D. R. Nelson, T. Piran, and S. Weinberg (World Scientific, Singapore, 1989).
[2] *Physics of Amphiphilic Layers*, edited by J. Meunier, D. Langevin, and N. Boccara (Springer-Verlag, Berlin, 1987).
[3] E. Evans and R. Skalak, *Thermodynamics of Biomembranes* (CRC, Boca Raton, 1980).
[4] P. Fromherz, Chem. Phys. Lett. **94**, 259 (1983).
[5] P. Fromherz, C. Rocker, and D. Ruppel, Faraday Discuss. Chem. Soc. **81**, 39 (1986).
[6] M. Mutz and D. Bensimon, Phys. Rev. A **43**, 4525 (1991).
[7] W. Helfrich, Z. Naturforsch. **28C**, 693 (1973); H. J. Deuling and W. Helfrich, J. Phys. (Paris) **37**, 1335 (1976).
[8] S. Svetina and B. Zeks, Biomed. Biochem. Acta **42**, 86 (1983).
[9] L. Miao, B. Fourcade, M. Rao, M. Wortis, and R. K. P. Zia, Phys. Rev. A **43**, 6843 (1991).
[10] U. Seifert, K. Berndl, and R. Lipowsky, Phys. Rev. A **44**, 1182 (1991).
[11] R. Grebe and M. Zuckermann, Biorheology **29**, 735 (1990).
[12] U. Seifert, Phys. Rev. Lett. **66**, 2404 (1991).
[13] S. Liebler, R. R. P. Singh, and M. E. Fisher, Phys. Rev. Lett. **59**, 1989 (1987); C. J. Camacho and M. E. Fisher, *ibid.* **65**, 9 (1990).
[14] C. J. Camacho, M. E. Fisher, and R. R. P. Singh, J. Chem. Phys. **94**, 5693 (1991).
[15] B. Duplantier, Phys. Rev. Lett. **42**, 493 (1990).
[16] D. H. Boal, Phys. Rev. A **43**, 6771 (1991).
[17] Y. Kantor, M. Kardar, and D. R. Nelson, Phys. Rev. Lett. **57**, 791 (1986).
[18] M. Plischke and D. H. Boal, Phys. Rev. A **38**, 4943 (1988).
[19] R. Lipowski and M. Girardet, Phys. Rev. Lett. **65**, 2893 (1990).
[20] A. Baumgartner and J. S. Ho, Phys. Rev. A **41**, 5747 (1990).
[21] S. Komura and A. Baumgartner, Phys. Rev. A **44**, 3511 (1991).
[22] D. M. Kroll and G. Gompper, Science **255**, 968 (1992).
[23] D. H. Boal and M. Rao, Phys. Rev. A **45**, 6947 (1992).
[24] S. T. Milner and S. A. Safran, Phys. Rev. A **36**, 4371 (1987).
[25] U. Glaus, J. Stat. Phys. **50**, 1141 (1988).
[26] J. Ambjorn, B. Durhuus, and J. Frohlich, Nucl. Phys. B **257**, 433 (1985); J. Ambjorn, B. Durhuus, and T. Jonsson, *ibid.* **330**, 509 (1990), and references therein.
[27] C. F. Baillie and D. A. Johnston, Phys. Lett. B **273**, 380 (1991).
[28] A. Polyakov, Phys. Lett. **103B**, 207 (1981).
[29] J. Schwarz, Phys. Rep. **89**, 223 (1982).
[30] V. A. Kazakov, Phys. Lett. **128B**, 316 (1983).
[31] D. J. Gross, Phys. Lett. **138B**, 185 (1984).
[32] For comparative work on microemulsions, see Ref. [24] and G. Gompper and M. Schick, Phys. Rev. Lett. **62**, 1647 (1989).
[33] S. A. Safran, P. Pincus, and D. Andelman, Science **248**, 354 (1990).
[34] U. Siefert, L. Miao, H.-G. Dobereiner, and M. Wortis, in

Structure and Conformation of Amphiphilic Membranes, edited by R. Lipowsky (Springer-Verlag, Berlin, in press).

[35] D. D. Lasic, Biochem. J. **256**, 1 (1988) and references therein.

[36] Self-avoiding branched polymer behavior is obtained for fluid membranes in Refs. [22] and [23], but not in Ref. [21]. In Ref. [23] it is argued that the connectivity algorithm used in Ref. [21] allows branched polymer scaling to be seen at much smaller N than it needed for Refs. [22] and [23].